REVIEW

Contribution of different factors in heat production in Yb^{3+}-doped fiber laser: a review

Maryam Karimi*
Nuclear Science and Technology Research Institute (NSTRI), Photonic and Quantum Technology Research School, Tehran, Iran

Abstract. The three important factors that affect the output power and temperature of fiber lasers (FLs) were investigated in a large mode area step-index FL under a high-power operation. Photodarkening (PD), quantum defect (QD), and background loss cause increases in the FLs temperature and reductions in beam quality, stability, and power. PD and background loss coefficients have different values for the signal (laser) or pump wavelength. But QD depends on the difference between the pump and the laser wavelength. By considering the PD attenuation in the rate equations, the effects of forward, backward, and bidirectional pump schemes on heat distribution agents were investigated. FL characters, including core and clad sizes, both side reflectors, and FL lengths in each heat generation agent, were studied in detail. © *2022 Society of Photo-Optical Instrumentation Engineers (SPIE)* [DOI: 10.1117/1.OE.61.11.110902]

Keywords: double clad fiber laser; thermal effects; ytterbium-doped fiber; heat distribution; photodarkening effect; and rate equation.

Paper 20220744V received Jul. 16, 2022; accepted for publication Oct. 17, 2022; published online Nov. 24, 2022.

1 Introduction

High-power lasers with a kW-level output have been developed over the past 30 years and have a wide range of applications in medicine, industry, and defense.[1] The use of ytterbium (Yb) in the glass host for designing a laser has been considered since 1962.[2] Yb^{3+}-doped fiberglass with a Ge codopant has broadband absorption and emission spectrum from 0.97 to 1.2 μm, so different kinds of power sources can be used in a wide choice of wavelengths.[3,4]

Kilowatt fiber laser (FL) is achieved by Yb^{3+}-doped fiber, which operates near 1 μm.[5] By increasing the effective area of the core, the output power of FLs and amplifiers is increased. Although the nonlinear effects are reduced in the large mode field diameter,[6,7] the large mode area (LMA) active fibers are used for the fabrication of high-power FLs and amplifiers in most cases,[8,9] with high-power causing nonlinear effects to appear in the environment. Using high-power laser diodes (LDs) and doping concentrations, the length of FL can be reduced, which is suitable for suppressing nonlinear effects. Commercial LMAs with 20-μm core and 400-μm clad are widely used in kW-level FL products, and increasing the core or cladding results in poor beam quality or connection problems, respectively. Photonic crystal fibers are suitable options for designing the LMA single-mode FLs.[10,11] The optical nonlinear effects, such as stimulated Raman scattering, stimulated Brillouin scattering, and self- or cross-phase modulation, can be used to make several types of equipment, such as Raman FLs (RFLs) or Brillouin FLs and amplifiers, wavelength laser tuning, nonlinear spectroscopy, frequency metrology, ultra-FLs, and emerging technologies that make quantum mechanical effects.[12] Mode instability (MI) as a thermal nonlinear phenomenon is a disturbing effect that has not been introduced in any application until now.[13] MI is suppressed with different methods to increase the output power and beam quality,[4,14] tailoring the Yb-ion distribution, shifting the pump or signal power, using the large first clad doped fiber, using different pump configurations,[15] or coiling the FL to decrease the higher-order mode.[15–17] Thermo-optic effects are an important factor for MI and lead to long-term running instability. When Yb-doped optical fiber (YDF) is pumped, the intrinsic quantum defect (QD) combined with color center absorption caused by photodarkening (PD) is doomed to

*Address all correspondence to Maryam Karimi, mykarimi@aeoi.org.ir

generate considerable redundant heat.[18] Different techniques can mitigate thermal effects, such as water cooling, thermoelectric cooling, and anti-Stokes fluorescence cooling.[19] Using RFLs instead of doped FLs reduces QD up to 95%.[20]

In previous works, different definitions of the heat source in FLs were classified, and their simulation results were compared with each other.[21] In this work, the PD loss is added to the rate equations as a power decreasing factor, and under these changes, the effect of cavity parameters, such as core and first clad sizes, laser length, and the reflectors at the end of FL in heat distribution, is investigated in the same bidirectional pump scheme. Also, in Ref. 22, the stretched exponential function was considered for PD phenomena to be the new attenuation phenomena in the rate equation. In previous works, the effect of some fiber laser characteristics on FL output has not been determined. This will be done in this article.

2 Background of Heat Source in FLs

Three main factors create heat in the fiber. Background loss, QD, and PD are the main reasons for the temperature enhancement discussed in this paper.

2.1 *Attenuation (Background Loss)*

Fiber absorption involves the direct transfer of energy from the propagating light to the fiber material, resulting in excitation, especially the dopant active center to a higher energy state. The fiber loss mainly includes absorption loss caused by the fiber itself or by impurities in the fiber, scattering loss caused by the interaction of the photons with the glass itself, and bending loss induced by physical stress on the fiber. Two main contributions to optical absorption in fiber optic glasses are intrinsic absorption of the base glass and extrinsic absorption from the impurities within the glass.

Fiber loss is often measured by the cut-back method. For the measurement, white light is often used as the broadband source.[23] The measurement of very high attenuation in optical fibers requires the handling of correspondingly short fiber samples. Fluorescence properties cause challenges in measuring the true value of attenuation in the doped optical fibers.[24] Various techniques are proposed to measure the attenuation in doped fiber optics, for example, the conventional cut-back method can measure Rayleigh loss besides absorption from the ground state.[23] So, in the conventional cut-back method, the absorption cross-section must be evaluated by the direct method.[25] Double or triple cut back can also characterize the main doped fiber parameters simultaneously using pseudoparameters.[26,27] Another technique is the twice perpendicular measurement method with strict time management.[24] From any mentioned techniques, the background loss must be determined in the pump and signal (laser) wavelength separately.

2.2 *Quantum Defect*

The QD is the energy difference between the pump and signal photons converted to heat.[28] The QD is defined as the difference in photon energies:[29]

$$Q_{\mathrm{QD}}(z) = h\upsilon_p(z) - h\upsilon_\ell(z) = h\upsilon_p(z)\left(1 - \frac{\lambda_p}{\lambda_\ell}\right). \tag{1}$$

The value of $1 - \lambda_p/\lambda_\ell$ is the figure-of-merit that quantifies heat generation in an active fiber, where λ_p and λ_ℓ are the pump and lasing wavelengths, respectively. The QD takes on a value between 0 and 1 and represents the fraction of pump power (in the quantum limit) lost to heat.[30] It is also often specified as a percentage of the pump photon energy, effectively using only the parentheses in the equation above. The QD is converted into heat through nonradiative relaxation.[19] The QD is one of the most important heat sources in gain fibers, which could result in serious thermal effects on FLs, such as the thermal lens effect, thermal MI, and additional noise.[20] The QD limits the conversion efficiency, but more importantly, it is the main source of thermal load in FLs.[31]

The Yb^{3+}-doped FL has fewer QDs and an energy depletion mechanism. Depending on the pumping scheme chosen, the output efficiency of an FL may be in the range 60% to 80%, with 8% to 12% lost in QDs, 5% to 10% in excess pump loss, 5% to 10% in excess signal loss, and 0.5% to 1% for nonoptimized cavity design.[32] In the Er^{3+}-doped laser devices, there has been a serious problem because of large QDs and thermal management.[32]

Several techniques have been proposed to decrease the QD in FLs. First, judicious selection of host glass in FLs, phosphorus (P)-doped fiber, reduces the QD.[30] Also, phosphosilicate fiber-based RFL has great potential in achieving ultralow QD high-power laser output.[31] Tandem pumping brings the pump and signal wavelengths closer together and reduces the QD.[30] Another option is using the RFLs. It has half the QD of the common LD-pumped Yb-doped FL.[20] Research shows that cladding-pumped RFL would be a promising solution for high-power FLs because it combines the advantages of RFLs, cladding pumping, and low heat production.[20]

2.3 *Photodarkening*

The PD loss is another heat source that depends on the pump and signal wavelengths, seed power, fiber core size, etc.[5,33,34] The PD effect, which is also called photochromic damage or photoinduced absorption (PIA), occurs when color centers are irradiated with light at certain wavelengths.[35] To measure PD, two common methods are proposed: (1) measuring the loss *in situ* of the transmission light during ion excitation[18] and (2) examining the long-term laser output power stability.[18]

PD in Yb-doped FLs is observed as degradation in output laser power over time, which limits the operational lifetime. The material aspects of PD have been given considerable attention during the last two decades.[36] PD takes place when the YDF is pumped at the Yb absorption band (916/976 nm) or irradiated under a visible wavelength of 488 nm.[37] PD increases the background loss from the ultraviolet (UV) to the near-infrared bands and causes the absorption of pump light.[38] Also, the PD-induced thermal load can cause a series of issues. It could change the refractive index of the optical fiber via the thermooptic effect, affecting the waveguide structure and thereby altering the bending loss of different modes.[39] More seriously, the thermal load induced by PD could distort the phase of the beam and aggravate the thermally induced refractive index grating, which could eventually trigger the occurrence of MI.[39] The mechanism of PD has not been determined yet; however, researchers have made great efforts to suppress PD.[39] The PD problem is typically overcome using LMA fibers, but even with these fibers, PIA has been observed.[40] The absorption occurs in the visible and near-infrared, originating from the creation of color centers in the silica network.[40] The rare earth (RE) ions doping technique, RE concentration, homogeneity, host material composition, defects, and impurities in YDF were widely accepted as the main causes of color centers and thus the PD effect.[18] Dopant high concentration cause to stimulate in ion-clustering, increases PD possibility. Different mechanisms have been proposed to explain the formation of color centers. This could be due to charge transfer, nonbridging oxygen holes, oxygen deficiency centers, Yb^{2+} ions, or even $Yb^{2+} - Yb^{3+}$ pairs.[41] Some dopants, such as aluminum with high concentration or aluminum–phosphor, can suppress the PD effect.[18,39,42] Optimizing the doping composition by codoping with cerium (Ce), P, Al, and Na ions into the fiber could inhibit PD to a certain extent.[39] Recently, a new method has been proposed to reduce the PD in FLs and amplifiers.[39,43,44] In this way, O_2- or H_2-loaded fiber exhibits excellent thermal performance in FLs.[39] Propagation loss (PL) in the pump and signal wavelengths also increases the temperature in the FLs and amplifiers.[33,45] The physical description of the PD effect is interpreted as the creation or existence of the color centers.[46–48] The color centers introduce additional absorption bands spread from UV to visible and have tailed the near-infrared,[46,49] where the pump and signal wavelengths are acted in the FL. In many doped fibers with the RE ions, such as Tm^{3+}, Ce^{3+}, Pr^{3+}, Er^{3+}, Tb^{3+}, and Yb^{3+}, the PD effect has been reported.[47,48] Different factors affect the PD phenomena. Claustration of Yb ions increases the PD effect.[46] Although Yb/Al codoped fiber has large absorption and emission cross-sections and proper thermal property, the level of PD is high.[50] Some codopants, such as Ce or P, in Yb/Al codoped fiber can be useful for decreasing the PD effects.[50,51] In both cases, the emission and absorption cross-sections of the doped fiber are reduced. To achieve the high gain, the Yb

concentration must be increased, which increases the PD loss, so the codopant concentration must be carefully selected to have a lower MI at high-power FL.[51]

3 Modeling of Heat Distribution in FL

The PD effect reduces the power of the signal (lasing) and pumps.[33,48] So, in high-power FLs and FAs where the PD effect is seen, an additional loss coefficient, such as PD loss, can be inserted as the power consumer at the rate equation. At low pump powers, the PD loss is negligible or near zero, but at high-power FLs, this excess loss is significant. Therefore, we expect that the PD loss coefficient depends on the beam power, so the coefficient value rapidly increases at a certain power value. Because the number of color centers in the sample should be limited, after the special power value, the PD loss coefficient must be reached at a constant limit.

The experimental results of the photobleaching (PB) loss variation with respect to the incidence power at 633 nm for different dopant concentration were represented.[38] Increasing the pump power causes an increase in PD loss in the sample. At 4 mW pump power, the loss approaches a constant value. In Ref. 39, PD-induced excess loss with and without H_2-loaded in the fiber is depicted. The PD loss occurs in the low-level pump power between 16 and 86 mW in the Yb-doped fiber.[37] In Refs. 39 and 52, a classical stretched exponential function is used to fit the time variation of the PD effect. The stretched exponential function in the form of $\alpha_{\mathrm{PD}-\lambda}(I_\lambda) = A(1-\exp(-\varepsilon I_\lambda))$ was considered for the PD loss with respect to input power,[27,53] where $\alpha_{\mathrm{PD}-\lambda}$ is the PD attenuation at a selected wavelength λ, I_λ is the input pump power, and the ε and A are constants with positive values. The results of the PB loss were fitted on the stretched exponential function. If the PD loss has a similar trend to the PB loss, the suggested function for the excess loss can be matched to the experimental reality. Nonetheless, the value of the $\alpha_{\mathrm{PD}-\lambda}$ can be considered to be a constant value in the small increments of power. In this paper, it was assumed that the value of the PD loss is constant at the considered pump value. The numerical solving of rate equations is the common method to investigate FL power variations,[54] and the rate equations are present in Ref. 21 and given as

$$\pm\frac{dP_\ell^{\pm}(z)}{dz} = \Gamma_\ell[(\sigma_\ell^e+\sigma_\ell^a)N_2(z)-\sigma_\ell^a N]P_\ell^{\pm}(z)-\alpha_\ell P_\ell^{\pm}(z), \tag{2}$$

$$\pm\frac{dP_p^{\pm}(z)}{dz} = -\Gamma_p[\sigma_p^a N-(\sigma_p^e+\sigma_p^a)N_2(z)]P_p^{\pm}(z)-\alpha_p P_p^{\pm}(z), \tag{3}$$

$$\frac{N_2(z)}{N} = \frac{\frac{[P_p^+(z)+P_p^-(z)]\sigma_p^a\Gamma_p}{h\upsilon_p A_{\mathrm{co}}}+\frac{[P_\ell^+(z)+P_\ell^-(z)]\sigma_\ell^a\Gamma_\ell}{h\upsilon_\ell A_{\mathrm{co}}}}{\frac{[P_p^+(z)+P_p^-(z)](\sigma_p^a+\sigma_p^e)\Gamma_p}{h\upsilon_p A_{\mathrm{co}}}+\frac{1}{\tau}+\frac{[P_\ell^+(z)+P_\ell^-(z)](\sigma_\ell^a+\sigma_\ell^e)\Gamma_\ell}{h\upsilon_\ell A_{\mathrm{co}}}}. \tag{4}$$

It should be noted that, in the normal case, the addition of α_{PD} in the equations is incorrect. The relationship is valid when the pump power is high enough that the PD effect is started. $P_p^{\pm}$ and $P_\ell^{\pm}$ are the (+, forward; −, backward) of the pump and lasing power, respectively. υ_p and υ_ℓ are the frequencies of the pump and lasing, respectively. σ_ℓ^e, σ_ℓ^a, and σ_p^a are emission and absorption cross-sections of the lasing and absorption cross-section of the pump power, respectively. h is Planck's constant, and τ is the steady-state lifetime. N is the dopant concentration in ion (m^3), and z is position along the fiber length. Γ_p and Γ_ℓ are the overlap factors at the pump and lasing wavelength, respectively. The overlap factor of the pump power in double-clad FL is estimated as $\Gamma_p \approx A_{\mathrm{co}}/A_{\mathrm{cl1}}$.[55,56] The overlap factor at the lasing wavelength is $\Gamma_\ell = 1-\exp(-2r_{\mathrm{co}}^2/\omega^2)$, where r_{co} is the radius of the FL core and ω is the spot size. For the Gaussian pulse shape with the V number in the range in the range of 0.8 to 2.8, the experimental relation approximate of the spot size in the doped fiber is used as follows:[21]

$$\omega = \rho\left(0.616+\frac{1.66}{V^{1.5}}+\frac{0.987}{V^6}\right). \tag{5}$$

α_p and α_ℓ are background losses at the pump and laser wavelength, respectively. α_{PD-p} and $\alpha_{PD-\ell}$ are PD losses at the pump and laser wavelength, respectively,[23,57] for which conventional FL is not considered in the rate equations. The PD loss coefficient depends on the dopant concentration and is determined as[23]

$$\alpha_{PD^{633\text{ nm}}}\ (\mathrm{dB/m}) \approx 175\left(\frac{N}{8.74\times10^{25}}\right)^{2.09}\cdot\frac{N_2/N}{0.46},$$
$$\alpha_{PD^{1\ \mu m}}\ (\mathrm{dB/m}) \approx 175\left(\frac{N}{\mathrm{AFF}\times8.74\times10^{25}}\right)^{2.09}\cdot\frac{N_2/N}{0.46}\cdot\frac{\mathrm{AFF}}{\gamma},$$
$$\gamma = 24.5, \mathrm{PD}^{633} = \frac{\mathrm{PD}^{1\ \mu m}}{\gamma}\left(\frac{\mathrm{dB}}{\mathrm{m}}\right), \tag{6}$$

where AFF is the area filling factor because the experimental results of PD loss are present in the visible region[46,49,57] and details of this loss in the pump and signal wavelength are not available. So, in this paper, it is assumed that $\alpha_{PD-\ell} \approx \alpha_{PD-p} \approx \alpha_{PD^{1\ \mu m}}$ because there are not enough experimental results to replace the real values.

The pump variations are determined independent of the signal (lasing) beam specifications as[3]

$$\frac{dP_p(z)}{dz} = -\frac{Ah\upsilon_p}{\phi_p\tau}N_2(z). \tag{7}$$

In Eq. (7), ϕ_p is the pump quantum efficiency, for which Yb^{3+} and $\phi_p \sim 1$.[3]

By combining Eqs. (2) and (7) and the integration of the equation, the pump power variations along the fiber length are expressed as follows:

$$\ln\frac{P_p^{\pm}(z)}{P_p^{\pm}(0)} + \frac{\phi_p\tau}{Ah\upsilon_p}\left[(\sigma_p^e+\sigma_p^a) - \frac{\ln 10}{10}\frac{C}{N}\right](P_p^{\pm}(z)-P_p^{\pm}(0)) + (\sigma_p^a N\Gamma_p+\alpha_p)z = 0,$$
$$C = 175\cdot\left(\frac{N}{\mathrm{AFF}\times8.74\times10^{25}}\right)^{2.09}\cdot\frac{\mathrm{AFF}}{0.46\gamma}. \tag{8}$$

The heat distribution equation in the core and clads region of the double-clad FL are described by the thermal conduction equation in the cylindrical coordinates[58,59]

$$\frac{1}{r}\frac{\partial}{\partial r}\left(r\frac{\partial T_{\mathrm{core}}(r,z)}{\partial r}\right) = -\frac{Q(z)}{K_1}, \quad (0\le r\le\in a), \tag{9}$$

$$\frac{1}{r}\frac{\partial}{\partial r}\left(r\frac{\partial T_{\mathrm{clads}}(r,z)}{\partial r}\right) = 0, \quad (a\le r\le c), \tag{10}$$

where $Q(r,z)$ is the heat density per unit of volume ($\mathrm{W/m^3}$). In this paper, it is assumed that the generated heat from the QD, PD, and background loss vary as follows:[23]

$$Q_T(z) = Q_{\mathrm{QD}}(z) + Q_{\mathrm{PD}}^P(z) + Q_{\mathrm{PD}}^\ell(z) + Q_{\mathrm{PL}}^p(z) + Q_{\mathrm{PL}}^\ell(z), \tag{11}$$

$$Q_{\mathrm{PL}-i}(z) = \frac{\alpha_i}{A_m^i}(P_i^+(z)+P_i^-(z));\ i=(s,p),$$
$$A_m^i\text{: mode area of the light (pump or signal)}$$
$$\alpha_i\text{: propagation of loss due to absorption and not scattering} \tag{12}$$

$$Q_{\mathrm{PD}}^i(z) = \frac{\Gamma_i Ln(10)PD^{1\ \mu m}}{10A_{\mathrm{co}}}(P_i^+(z)+P_i^-(z)), \tag{13}$$

$$Q_{\mathrm{QD}}(z) = (1-S)\frac{\Gamma_p(\sigma_p^aN_1(z)-\sigma_p^eN_2(z))(P_p^+(z)+P_p^-(z))}{A_{\mathrm{co}}};\quad S=\lambda_p/\lambda_\ell. \tag{14}$$

where T_{core} and T_{clad} are the temperature variations at the core and clad, respectively. Q_{QD}, Q_{PD}^{p}, Q_{PD}^{ℓ}, Q_{PL}^{p}, and Q_{PL}^{ℓ} are the heat produced from QDs, PD at pump power, PD at laser (signal) power, PL at pump wavelength, and PL at laser (signal) wavelength, respectively. S is the quantum efficiency or optical conversion efficiency, which is λ_p/λ_ℓ. For the cladding regions $a \le r \le c$, there is no heat source, and $Q(z) = 0$. r is the radial coordinate, z is the longitudinal coordinate along the fiber, and K_1 is the thermal conductivity of silica. The thermal conductivity can have different coefficients for the core and the first and second clads of the fiber. Heat is only created in the doped core region of the FL. T_{core} and T_{clads} are the temperatures in the core and cladding regions, respectively. The temperature and its derivatives must be continuous across the inner boundaries. Moreover, at the outer cladding–air interface, heat is transferred by convective and radiative heat flux.[60,61] So, at the boundaries, the following conditions are confirmed:[21]

$$dT_{\text{core}}(r=0,z)/dr = 0 \rightarrow T_{\text{core}}(r=0,z) = \text{cte}, \tag{15}$$

$$T_{\text{core}}(a,z) = T_{\text{clad1}}(a,z), \quad K_1 \frac{dT_{\text{core}}(r=a,z)}{dr} = K_2 \frac{dT_{\text{clad1}}(r=a,z)}{dr}, \tag{16}$$

$$T_{\text{clad1}}(b,z) = T_{\text{clad2}}(b,z), \quad K_2 \frac{dT_{\text{clad1}}(r=b,z)}{dr} = K_3 \frac{dT_{\text{clad2}}(r=b,z)}{dr}, \tag{17}$$

$$\frac{dT_{\text{clad2}}(r=c,z)}{dr} = \frac{h}{K_h}(T_c(r,z) - T_{\text{clad2}}(r=c,z)) + \frac{\sigma_b \varepsilon}{K_h}(T_c^4(r,z) - T_{\text{clad2}}^4(r=c,z)), \tag{18}$$

where h is the heat transfer coefficient, which depends on the environmental temperature.[62] In this paper, by assuming a constant value for the environmental temperature, a constant value is considered for heat transfer coefficient. The values of K_1, K_2, and K_3 are the conductive heat transfer coefficients at the core and first and second clads, respectively. K_h is the conductive heat transfer coefficients of the air. T_{core}, T_{clad1}, and T_{clad2} are the temperature variations in the core and first and second clads, respectively. T_c is the environment temperature or the temperature that the FL sustains. σ_b is the Stefan–Boltzmann constant, and ε is the surface emissivity. Equations (11) and (12) both consist of two boundary conditions (the temperature and its derivative are continuous at the boundaries), so there are six boundary conditions that determine all of the constant values. By solving Eqs. (9) and (10) using the boundary conditions, the value of T_{clad2} at the radial point $r = c$ is obtained as follows:[21]

$$f(T_{\text{clad2}}(r=c,z)) = \frac{\sigma_b \varepsilon}{K_h} T_{\text{clad2}}^4(r=c,z) + \frac{h}{K_h} T_{\text{clad2}}(r=c,z) - \frac{\sigma_b \varepsilon}{K_h} T_c^4 - \frac{h}{K_h} T_c + \frac{Q(z)a^2}{2K_3 c} = 0. \tag{19}$$

So, the temperature changes in the core and clads are as follows:[21]

$$T_{\text{core}}(r,z) = T_0(z) - \frac{Q(z)r^2}{4K_1} \quad (0 \le r \le a), \tag{20}$$

$$T_{\text{clad1}}(r,z) = -\frac{Q(z)a^2}{K_2} \ln r + Q(z)a^2 \ln b\left(\frac{1}{k_2} - \frac{1}{k_3}\right) + T_{\text{clad2}}(r=c,z) + \frac{Q(z)a^2}{K_3} \ln c \quad (a \le r \le b), \tag{21}$$

$$T_{\text{clad2}}(r,z) = -\frac{Q(z)a^2}{K_3} \ln r + \frac{Q(z)a^2}{K_3} \ln c + T_{\text{clad2}}(r=c,z) \quad (b \le r \le c). \tag{22}$$

In previous work, the heat distribution of the double-clad FL with the bidirectional pump scheme was simulated by considering different definitions of the heat source at the FL, and the share of each factor in heat generation at the double-clad FL with the relatively large first clad size was determined.[21]

4 Simulation Results and Discussions

In Eq. (7), the refractive index of the glass with 6% mole GeO_2 ($x = 6\%$) is determined to be 1.4583 for the signal wavelength 1090 nm. The pump and lasing wavelengths are $\lambda_p = 925$ nm and $\lambda_\ell = 1090$ nm, respectively. There is no Bragg reflector at the pump wavelength $R3 = 0$. The values of the simulation parameters, such as cross-sections, first and second clad radiuses, steady-state lifetime, background losses, input pump power, etc., are given in Table 1.

The variations of the pump and signal power with respect to position along the FL for different pump schemes are depicted in Figs. 1(a1)–1(c1). As shown in Figs. 1(a1)–1(c1), pump power is exponentially decreasing, according to Eq. (8), in all pump schemes. The laser output power depends on the summation of input pump powers.

In Figs. 1(a2)–1(c2), all normalized generated heat with respect to the FL position is shown. Different heat sources include PD in the pump and signal wavelength, PL or background loss at the pump and signal wavelength, and the QD. The heat generated by each of the heat generating agents, along with the FL, has different values as $R_{co} = 15$ μm. For the bidirectional pump scheme, the heat generated by PD (s) and PL (s) has the maximum values in the middle of the FL and the minimum amount at both sides of the FL, whereas the heat generated by the QD has the maximum amount at both ends of the FL and the minimum at the midpoint of the FL.

In the side pump schemes (forward and backward), the heat generated by the QD has the maximum value at the pump entrance regions, and the heat generated by the PL (s) has a minimum value at the pump entrance regions. In general, for all pump schemes, the Q_{QD} has the highest amount, and Q^{ℓ}_{PL} and Q^{ℓ}_{PD} have the lowest amounts at the pump entrance regions. In all pump schemes, Q^{p}_{PL} and Q^{p}_{PD} have negligible values and can be ignored.

Figures 1(a1)–1(c1) show the mean values of different heat-generated factors in three pump schemes. The mean normalized value of each heating factor in the FL is defined as $\sum_{i=1}^{N} Q_i/N$. As shown in Figs. 1(a1)–1(c1), Q^{ℓ}_{PD} has a higher percentage of the heating agent in the

Table 1 Parameter values used in the heat distribution simulation of Yb double-clad FL.

Parameters	Values	Parameters	Values
Emissivity	$\varepsilon = 0.85$	Stefan–Boltzmann constant	$\sigma_b = 5.67 \times 10^{-8}$ W/$(m^2 \cdot K^4)$
Ambient temperature	$T_c = 290$ K	Core conductive heat transfer coefficient	$K_1 = 1.38$
Laser wavelength (λ_i)	$\lambda_i = 1090$ nm	First clad conductive heat transfer coefficient	$K_2 = 1.38$
Signal background loss	$\alpha_S = 5$ dB/km	Second clad conductive heat transfer coefficient	$K_3 = 0.2$
Pump wavelength	$\lambda_p = 925$ nm	Air conductive heat transfer coefficients	$K_h = 0.025$ $Wm^{-1}K^{-1}$
Pump background loss	$\alpha_P = 3$ dB/km	Convective heat transfer coefficient	$H = 100$ $Wm^{-2}K^{-1}$
Power filling factor	0.0025	Laser absorption cross-section[21]	$\sigma^a_s = 1.23 \times 10^{-28}$ m^2
Steady-state lifetime	$T = 0.84$ s	Laser emission cross-section[21]	$\sigma^e_s = 1.24 \times 10^{-25}$ m^2
Dopant concentration	$N_t = 4 \times 10^{25}$ ion/m^3	Pump absorption cross-section[21]	$\sigma^a_p = 6.64 \times 10^{-25}$ m^2
Active fiber length	$L = 20$ m	Pump emission cross-section[21]	$\sigma^e_p = 4 \times 10^{-26}$ m^2
Front Bragg reflector	$R_1 = 0.98$ at 1090 nm	Input pump power, FWP, and BDP	$P_p = 500$ and 250 mW
Back Bragg reflector	$R_2 = 0.4$ at 1090 nm	Input pump power, BWP, and BDP	$P_p = 500$ and 250 mW

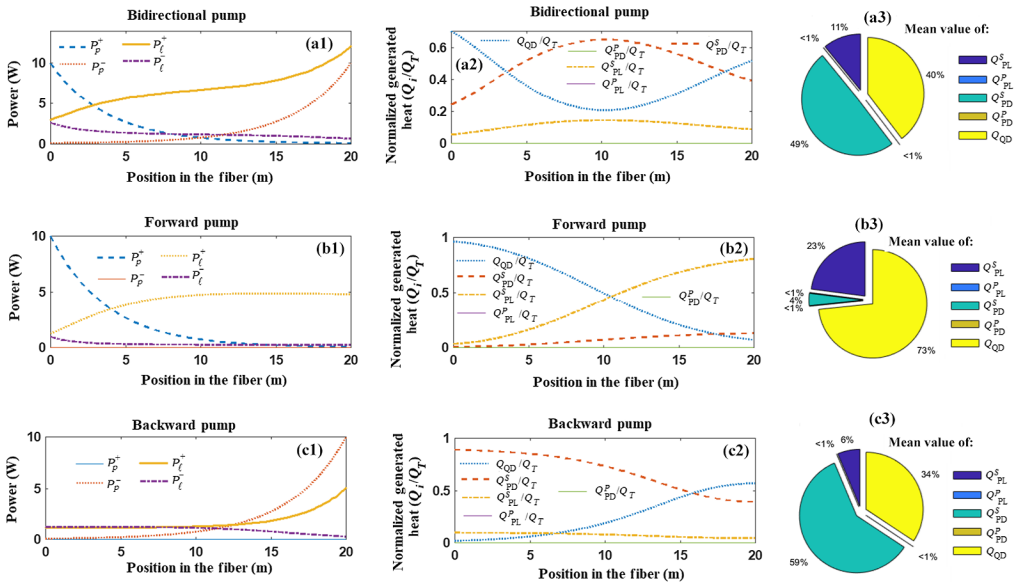

Fig. 1 (a1)–(c1) Pump and signal variations with respect to the position in the FL, (a2)–(c2) normalized generated heat with respect to the position in the FL, and (a3)–(c3) mean value of heat generated in the FL from different heating factors.

bidirectional and backward pump (BWP) schemes and a lower percentage in the forward ones. Q_{QD} is the main factor of the heating agent in the forward pump (FWP) scheme.

The effect of core size on heat generation in the FL is investigated in Fig. 2. The dopant density is assumed to be constant in each core size. Therefore, the number of dopants in the bigger core size is larger. So, to have a constant value for density in the calculations, the value of N is multiplied by r_{co}^2/r_{clad1}^2. As shown in Fig. 2(a), by increasing the core size, the value of PD-generated heat Q_{PD}^{ℓ} is increased. In other words, in the larger core sizes, the PD heat is the main reason for the increase in the FL temperature. According to Eq. (13), the QD heat is inversely proportional to the core area. In comparison with two FLs with different core sizes and equal pump power, the pump power is rapidly absorbed in the input ends of the FL with the larger core area. So, it is expected that, in the FL with the larger core, the middle points of FL have lower pump levels and consequently lower heat generation from the QD effect, which Fig. 2(a) confirms.

According to Eq. (11), the PL heat generation is inversely proportional to the mode area and depends directly on the signal (laser) power. In the FL, the signal (laser) output is directly related

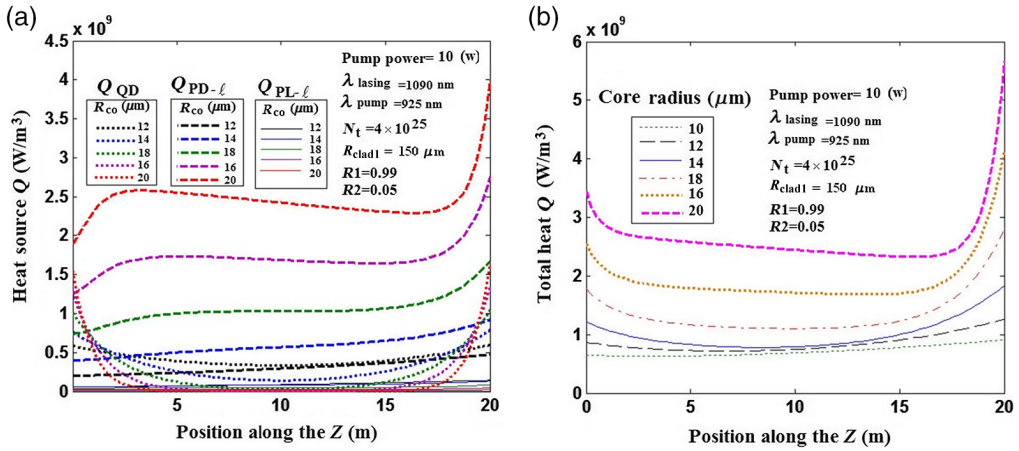

Fig. 2 Heat variation along with the fiber position: (a) share of QD, PD-ℓ, and PL-ℓ in heat generation for different core sizes and (b) total heat variation versus FL position for different core sizes.

to the pump power value. So, in the FLs with equal pump power, the laser output cannot grow from a certain level. By increasing the core radius, the mode area increases. As shown in Fig. 2(a), by increasing the core size, the value of the Q^{ℓ}_{PL} is reduced, but the magnitude of this change is negligible. Figure 2(b) shows the evolution of total heat generation versus core size. By increasing the core radius, more heat is generated at the ends of FL; so, in the FL with the larger core size, the probability of FL damage is higher at the output of the FL due to the higher temperature.

In Fig. 3, the core size effect on heat generation was investigated in the FL with a bidirectional pump scheme. In this paper, it is assumed that the dopant concentration in the FL core is constant. In other words, by increasing the core size, the value of the "N_t" increases by the square of the core size. As shown in Fig. 3, for an FL with a small core, the main factor of heat generation is the QD. So, in the FL with $R_{\mathrm{co}} = 10$ μm, 68% of the generated heat is created by the QD agent. By increasing the core size, the share of the QD and the PL decreases in heat generation. So, in the FL with $R_{\mathrm{co}} = 20$ μm, 10% of the generated heat is created with the QD agent. For the FL with a large core, the main heat generation factor is the PD. In the FL with $R_{\mathrm{co}} = 20$ μm, 88% of the generated heat is created by the PD agent. In general, by increasing the core size, Q^{ℓ}_{PL} and Q_{QD} are decreased, and Q^{ℓ}_{PD} is increased. In Fig. 3, due to the negligible effect of Q^{P}_{PD} and Q^{p}_{PL}, both of them are ignored.

In Fig. 4, simultaneously, the effects of the FL core and first clad sizes on each heat-producing factor in the FL with a backward pump scheme are investigated as a percentage graph. As shown in Fig. 4, from left to right, the core size changes by 10, 15, and 20 μm.

As shown in Fig. 4, by increasing the core size, the value of the Q^{ℓ}_{PD} increases and the Q_{QD} and Q^{ℓ}_{PL} decrease. The variation procedure of the heat generation sources is similar to the bidirectional pump scheme. Figure 4 shows that, in the backward pump scheme similar to the bidirectional pump, the effect of the Q^{P}_{PD} and Q^{p}_{PL} is negligible and can be ignored. The graph's variation from up to down shows the heat generation source variations in FLs with the first clads changing from 100 to 200 μm. The first clad of the FL only affects the pump overlap factor Γ_p. Increasing the first clad of the FL causes a decrease in the Γ_p value. Increasing the first clad is approximately equivalent to decreasing the pump power. The effect of increasing the first clad size exactly is opposite the effect of increasing the core size on the heat generation factors. As shown in Fig. 4, by increasing the first clad of the FL, the Q_{QD} and Q^{ℓ}_{PL} increase, and the Q^{ℓ}_{PD} decreases.

The effect of the front Bragg reflector ($R1$) on the forward and backward signal (laser) power, different heat generation factors, and value of the $\alpha_{\mathrm{PD}-\ell}$ for different pump schemes are depicted in Fig. 5. In all pump schemes, increasing the $R1$ value causes an increase in the forward pump power value (laser output), but the variation of backward laser power is negligible and can be ignored. Figures 5(a2)–5(c2) show the variation of the different heat-generating agents with

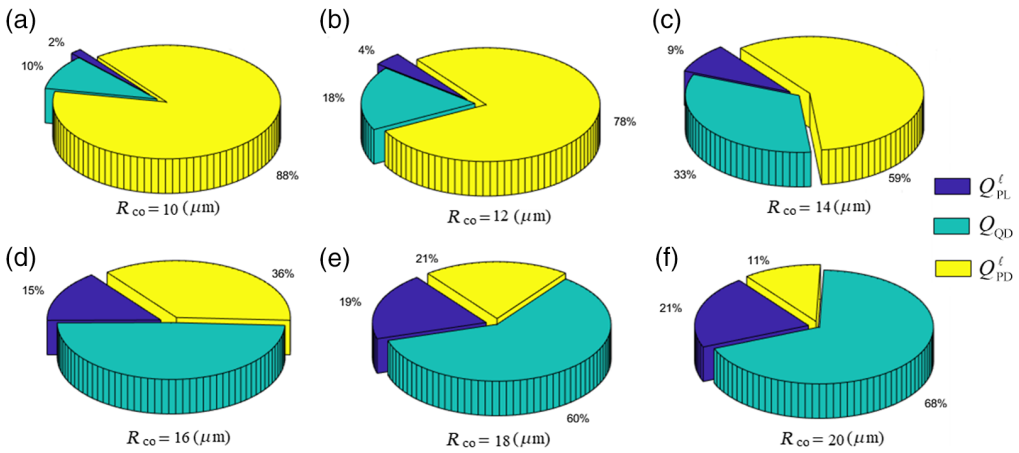

Fig. 3 (a)–(f) Mean heat generated percentage for different heat sources for various core sizes in the FL with a bidirectional pump scheme.

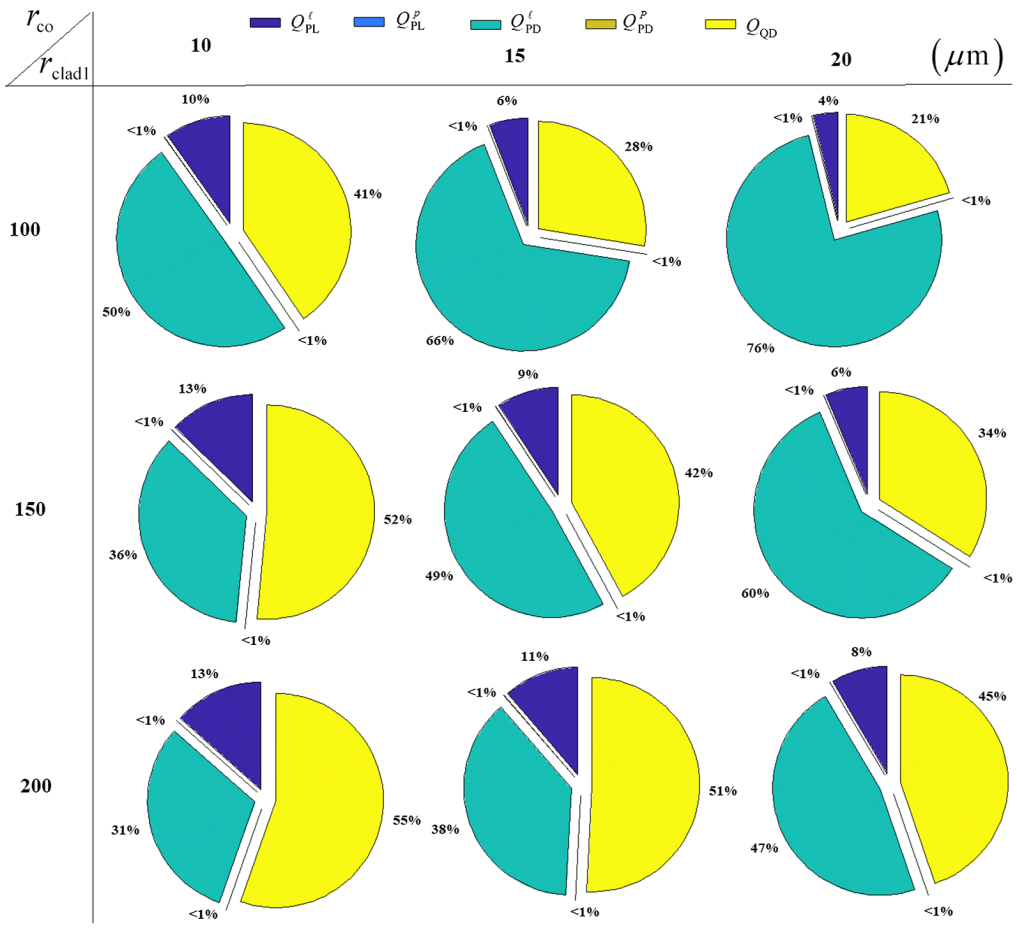

Fig. 4 Heat generated percentage with the different heat sources for various core and first clad sizes in the FL with backward pump scheme.

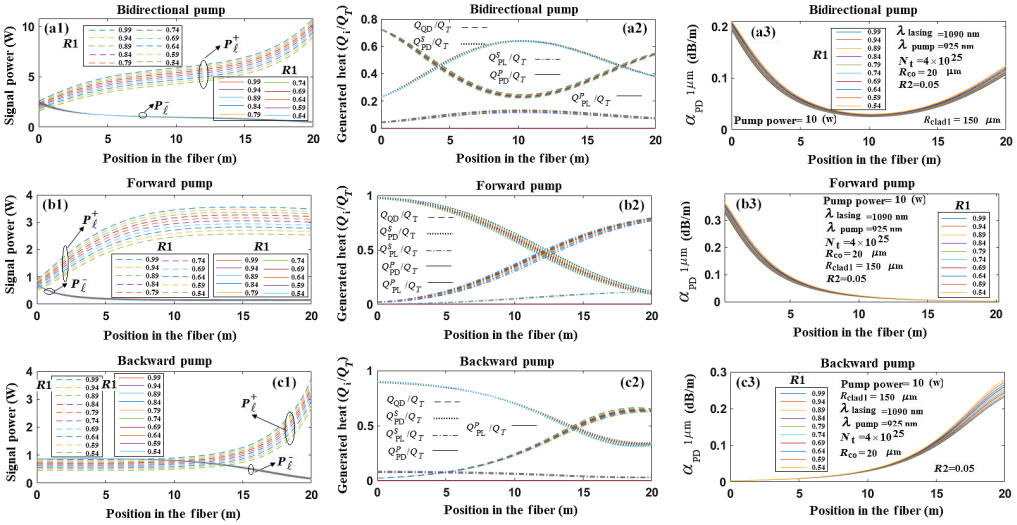

Fig. 5 Effect of the front Bragg reflector ($R1$) on: (a1)–(c1) signal power, (a2)–(c2) different heat generation factors, and (a3)–(c3) the value of $\alpha_{PD\text{-}\ell}$ with different pump schemes.

respect to the FL length for different $R1$ values and pump schemes. By decreasing the $R1$ value from 0.99 to 0.54, the values of the Q^{ℓ}_{PL} and Q^{ℓ}_{PD} decrease, but the Q_{QD} increases. The sensitivity of the heat-generating factors to the $R1$ value is small. The variation of the $\alpha_{\mathrm{PD}-\ell}$ in Figs. 5(a3)–5(c3) shows that maximum changes have been happening on the pump input side. By decreasing the $R1$ value, the value of $\alpha_{\mathrm{PD}-\ell}$ increases.

Figures 6(a1)–6(c1) show the total heat generated variation with respect to the FL position for different values of the back Bragg reflector ($R2$) in different pump schemes. In all pump schemes, the maximum variation in the heat generation occurs at the input point of the FL. In the comparison of Figs. 6(a1)–6(c1), it is clear that, in the forward pump scheme, the variation of generated heat has a negligible variation with the $R2$ coefficient. The backward pump scheme shows significant variation in the heat generation by the $R2$ variation. In all pump schemes, increasing $R2$ values causes an increase in heat generation at all points of the FL. Figures 6(a2)–6(c2) show different heat-generating agents. As shown in Figs. 6(a2)–6(c2), in all pump schemes, $R2$ has maximum effects on Q^{ℓ}_{PD}. The effect of the $R2$ variation on the other heating factors is negligible and can be ignored. In the BWP scheme, the variation in Q^{ℓ}_{PD} is relatively considerable by decreasing the R2 value, causing a decrease in the Q^{ℓ}_{PD} amount. Figures 6(a3)–6(c3) show the heat generated percentage for different heat sources at $R2 = 0.005$. In comparing Fig. 1(a3) with Fig. 6(a3), it is observed that, by decreasing the $R2$ value, the Q_{QD} does not remarkably change and the value of Q^{ℓ}_{PL} decreases and Q^{ℓ}_{PD} increases. In comparing Fig. 1(b3) with Fig. 6(b3), by decreasing the $R2$ value, the share of Q^{ℓ}_{PD} in heat generation decreases to <1%, and the share of Q_{QD} increases up to 94%. As shown in Figs. 1(c3) and 6(c3), decreasing the $R2$ value causes a decrease in Q^{ℓ}_{PD} and Q^{ℓ}_{PD} and an increase in Q_{QD} simultaneously.

In Fig. 7, the total generated heat in FLs with different cavity lengths and pump schemes is investigated. In the bisectional pump scheme, the laser pump has 10 W on each side. But, in the forward or backward pump scheme, only 10 W pump power arrives from one side of the laser. So, it is expected that, in the bisectional pump scheme the generated heat has a higher value with respect to the two other schemes. Figure 7(a) confirms this expectation. In the bidirectional and backward pump schemes, FL has high heat generation, and with an increasing FL length, the generated heat changes slightly. These small changes are descending on the bidirectional and

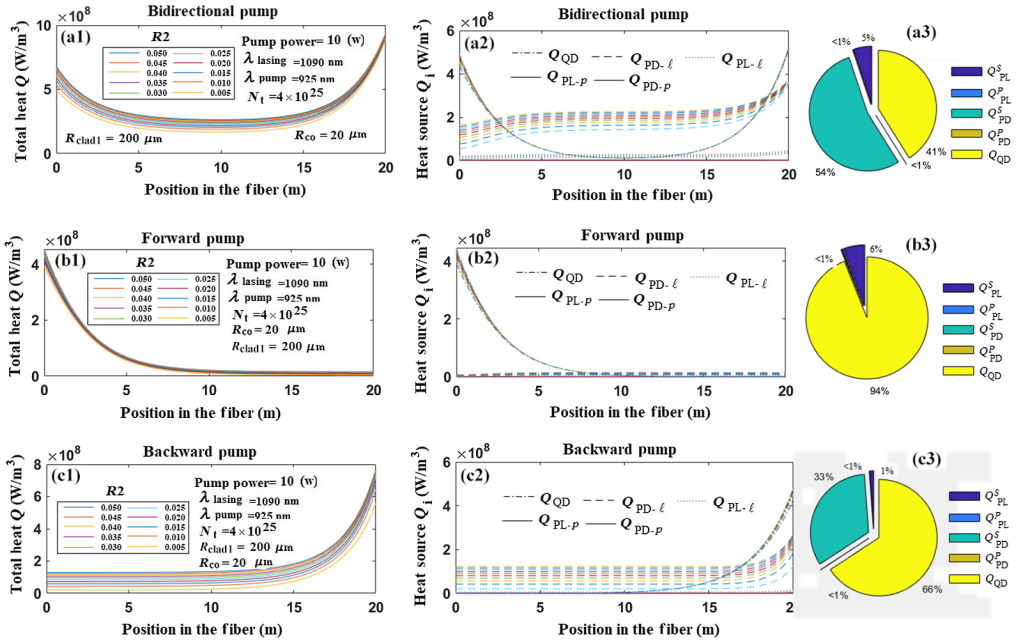

Fig. 6 Effect of the back Bragg reflector ($R2$) on: (a1)–(c1) total generated heat, (a2)–(c2) the different heat generation sources with respect to fiber position, and (a3)–(c3) the heat generated percentage with the different heat sources and the different pump schemes.

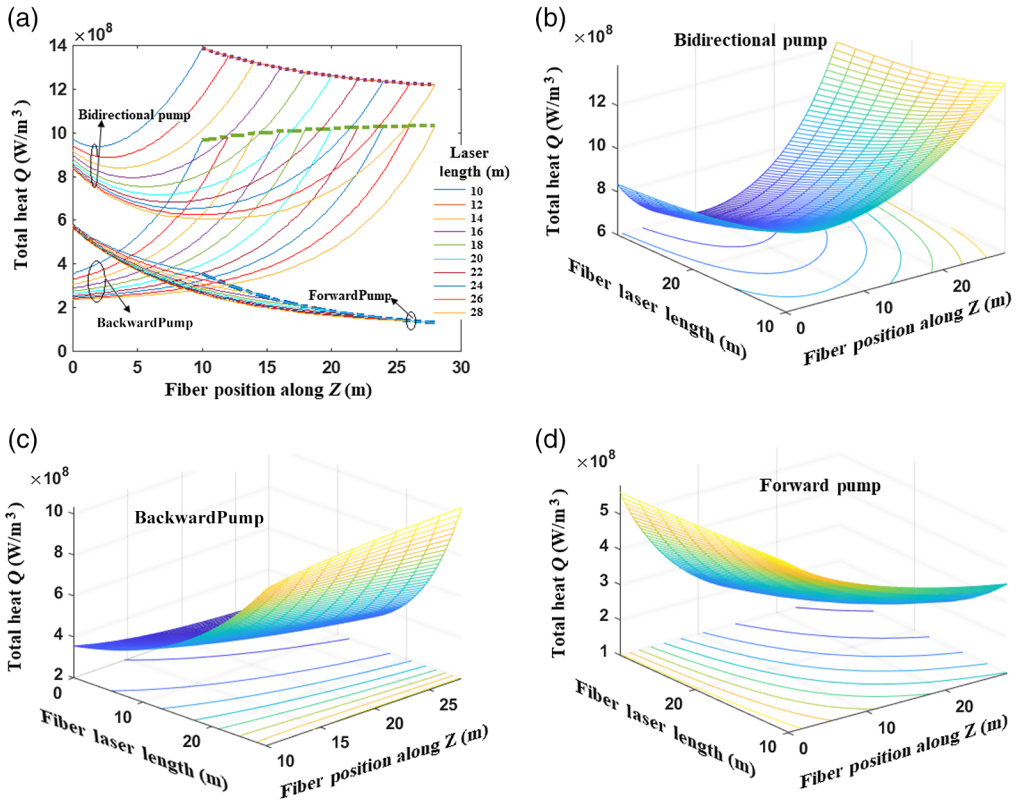

Fig. 7 (a) Total heat variation with respect to the FL position in the FLs with the different lengths and pump schemes, 3D variation of the total heat with respect to the laser length, and the FL position; (b) bidirectional pump scheme; (c) backward pump scheme; and (d) forward pump scheme.

ascending on the backward pump schemes. In the forward pump scheme, the input point of the FL has a maximum temperature that does not depend on the FL length. At the endpoint of the FL in this scheme, by increasing the FL length, the heat generation decreases. The 3D variations of heat generation with respect to the FL position and FL length for the bidirectional, backward, and forward pump schemes are depicted in Figs. 7(b)–7(d), respectively.

5 Conclusion

This paper is dedicated to the continuation of the previous simulation on heat distribution in FLs. The purpose of this paper is to investigate the effect of FL characters, such as core, clad, and FL length sizes, and pump schemes on the heat distribution.

It was shown that the pump input points in any pump scheme design generate the highest heat amount in FL. Also, it was shown that the contribution of Q_{PD}^{P} and Q_{PL}^{p} in heat generation is negligible and can be ignored.

In the bidirectional pump scheme, Q_{PD}^{ℓ} has the highest share, and Q_{PL}^{ℓ} has the lowest share in heat generation in the FL. In the forward pump scheme, Q_{QD} has the highest share, and Q_{PD}^{ℓ} has the lowest share in heat generation in the FL. In the backward pump scheme, similar to the bidirectional one, Q_{PD}^{ℓ} has the highest share, and Q_{PL}^{ℓ} has the lowest share in heat generation in the FL.

In this paper, the effect of core size in the FL with a bidirectional pump scheme on the heat distribution was investigated. It was shown that, in the FL with a small core, Q_{PD}^{ℓ} is the most exothermic factor. By increasing the core size, the share of Q_{PD}^{ℓ} in heat generation decreases, and the shares of Q_{PL}^{ℓ} and Q_{QD} increase, so in the FL with the core radius $= 10$ μm, the share of Q_{PD}^{ℓ} in heat generation is 85% and in the FL with core radius $= 20$ μm, the share is 85%.

The effect of the first clad size on heat distribution was investigated, and it was shown that by increasing the first clad size, the share of Q_{QD} in heat generation was increased, and the share of Q_{PD}^{ℓ} was decreased. The variation of Q_{PL}^{ℓ} was increasing with a slight slope.

In this paper, the effects of the first and second Bragg reflector coefficients on heat generation were investigated. The variation of $R1$ has a negligible effect on the heat distribution. The second Bragg reflector $R2$ also has little effect on heat distribution. Simulation shows that this parameter can change the value of Q_{PD}^{ℓ}.

The effect of the FL length on heat distribution depends on the pump scheme. In the backward pump scheme, by increasing the FL length, the generated heat value increases at the end of the FL (pump input) with a slight slope. In the forward and bidirectional pump schemes, the heat generation, as well as the temperature at the end of the FL, decreases with the FL length. This variation has a slight slope in the bidirectional pump scheme.

References

1. M. N. Zervas and C. A. Codemard, "High power fiber lasers: a review," *IEEE J. Sel. Top. Quantum Electron.* **20**(5), 219–241 (2014).
2. H. W. Etzel, H. W. Candy, and R. J. Ginther, "Stimulated emission of infrared radiation from ytterbium activated silicate glass," *Appl. Opt.* **1**, 534 (1962).
3. H. M. Pask et al., "Ytterbium-doped silica fiber lasers: versatile sources for the 1–1.2 pm region," *IEEE J. Sel. Top. Quantum Electron.* **1**, 2–13 (1995).
4. J. Oewiderski et al., "Rare-earth-doped high-power fiber lasers generating in near infrared range," *Opto-Electron. Rev.* **12**(2), 169–173 (2004).
5. A. V. Smith and J. J. Smith, "Mode instability thresholds for Tm-doped fiber amplifiers pumped at 790 nm," *Opt. Express* **24**, 975–992 (2016).
6. C. Jauregui et al., "Temperature induced index gratings and their impact on mode instabilities in high-power fiber laser systems," *Opt. Express* **20**, 440–451 (2011).
7. C. Jauregui, J. Limpert, and A. Tünnermann, "Derivation of Raman threshold formulas for CW double-clad fiber amplifiers," *Opt. Express* **17**, 8476–8490 (2009).
8. S. Ramachandran et al., "Ultra-large effective area, higher-order mode fibers: a new strategy for high-power lasers," *Laser Photonics Rev.* **2**, 429–448 (2008).
9. N. G. R. Broderick et al., "Large mode area fibers for high power applications," *Opt. Fiber Technol.* **5**, 185–196 (1999).
10. S. Saitoh et al., "Design optimization of large-mode-area all-solid photonic bandgap fibers for high-power laser applications," *J. Lightwave Technol.* **32**, 440–449 (2014).
11. K. Li et al., "High power single-mode large-mode-area photonic crystal fiber laser with improved Fabry-Perot cavity," *Chin. Opt. Lett.* **4**, 522–524 (2006).
12. G. P. Agrawal, *Applications of Nonlinear Fiber Optics*, 2nd ed., Academic Press (2008).
13. Z. Li et al., "Experimental demonstration of transverse mode instability enhancement by a counter-pumped scheme in a 2 kW all-fiberized laser," *Photonics Res.* **5**, 77–81 (2017).
14. K. H. Lee et al., "Transverse mode instability induced by stimulated Brillouin scattering in a pulsed single-frequency large-core fiber amplifier," *App. Opt.* **54**, 189–194 (2015).
15. R. Tao et al., "Dynamic characteristics of stimulated Raman scattering in high power fiber amplifiers in the presence of mode instabilities," *Opt. Express.* **26**, 25095–25110 (2018).
16. I. O. Zolotovskii et al., "Generation of sub picosecond pulses due to the development of modulation instability of whispering-gallery-mode wave packets in an optical waveguide with a travelling refractive-index wave," *Quantum Electron.* **48**, 818–822 (2018).
17. J. P. Koplow, D. A. V. Kliner, and L. Goldberg, "Single-mode operation of a coiled multimode fiber amplifier," *Opt. Lett.* **25**, 442–444 (2000).
18. S. Liu et al., "3 kW 20/400 Yb-doped aluminophosphosilicate fiber with high stability," *IEEE. Photonics J.* **10**, 1503408 (2018).
19. J. M. Knall et al., "A radiation-balanced silica fiber amplifier," *Phys. Rev. Lett.* **127**, 013903 (2022).
20. X. Ma et al., "Cladding-pumped Raman fiber laser with 0.78% quantum defect enabled by phosphorus-doped fiber," *High Power Laser Sci. Eng.* **10**, 1–16 (2022).

21. M. Karimi, "Theoretical study of the thermal distribution in Yb-doped double-clad fiber laser by considering different heat sources," *Prog. Electromagn. Res. C* **88**, 59–76 (2018).
22. M. Karimi, "Heat distribution in high power Yb doped fiber laser by considering photo-darkening effect," *MISCJ* **53**, 137–151 (2022).
23. G. Xiao et al., "Measurement of active optical fibers," in *Handbook of Optical Fibers*, pp 1–38, Springer, Singapore (2019).
24. A. Schwuchow et al., "Advanced attenuation and fluorescence measurement methods in the investigation of photodarkening and related properties of ytterbium-doped fibers," *Appl. Opt.* **53**, 1466–1473 (2014).
25. E. Desurvire, *Erbium Doped Fiber Amplifiers: Principles and Applications*, John Wiley & Sons Inc. (1994).
26. M. Karimi and F. E. Seraji, "A novel method for simultaneous measurement of doped optical fiber parameters," *Eur. Phys. J. Appl. Phys.* **50**, 20701 (2010).
27. M. Karimi and F. E. Seraji, "Experimental technique for simultaneous measurement of absorption-, emission cross-sections, and background loss coefficient in doped optical fibers," *Appl. Phys. B* **98**, 113–117 (2010).
28. J. W. Dawson et al., "Analysis of the scalability of diffraction limited fiber lasers and amplifiers to high average power," *Opt. Express* **16**, 13240–13266 (2008).
29. G. Nemova, "Radiation-balanced lasers: history, status, potential," *Appl. Sci.* **11**, 7539 (2021).
30. N. Yu et al., "Less than 1% quantum defect fiber lasers via ytterbium-doped multicomponent fluorosilicate optical fiber," *Opt. Lett.* **43**, 3096–3099 (2018).
31. Y. Zhang et al., "Phosphosilicate fiber-based low quantum defect Raman fiber laser with ultrahigh spectral purity," *Nanomaterials* **12**, 1490 (2022).
32. A. Jha, *Inorganic Glasses for Photonics*, John Wiley & Sons (2016).
33. C. Jauregui et al., "Simplified modelling the mode instability threshold of high-power fiber amplifiers in the presence of photodarkening," *Opt. Express* **23**, 20203–20218 (2015).
34. B. Ward, "Theory and modeling of photodarkening induced quasi static degradation in fiber amplifiers," *Opt. Express.* **24**, 3488–3501 (2016).
35. C. Ye et al., "Short-term and long-term stability in ytterbium-doped high-power fiber lasers and amplifiers," *IEEE. J. Sel. Top. Quantum Electron.* **20**, 0903512 (2014).
36. M. Engholm et al., "On the origin of photodarkening resistance in Yb-doped silica fibers with high aluminum concentration," *Opt. Mater. Express* **11**, 115–125 (2021).
37. H. Z. Li et al., "Pump wavelength dependence of photodarkening in Yb-doped fibers," *J. Lightwave Technol.* **35**, 2535–2540 (2017).
38. R. Cao et al., "532 nm pump induced photo-darkening inhibition and photo-bleaching in high power Yb-doped fiber amplifiers," *Opt. Express*, **27**, 26523–26531 (2019).
39. R. Cao et al., "Effective suppression of the photodarkening effect in high-power Yb-doped fiber amplifiers by H2 loading," *Photonics Res.* **8**, 288–295 (2020).
40. R. Peretti, C. Gonnet, and A. M. Jurdyc, "A new vision of photodarkening in Yb^{3+}-doped fibers," *Proc. SPIE* **8257**, 825705 (2012).
41. R. Peretti, C. Gonnet, and A. M. Jurdyc, "Revisiting literature observations on photodarkening in Yb^{3+}-doped fiber considering the possible presence of Tm impurities," *App. Phys.* **112**, 093511 (2012).
42. R. Sidharthan et al., "Photo darkening suppression in highly Yb-doped Aluminophosphosilicate fiber by addition of cerium," in *IEEE Conf. Lasers and Electro-Opt. Europe (CLEO EUROPE)*, pp. 23–27 (2019).
43. R. Cao, G. Chen, and J. Li, "Eliminating photodarkening effect by H2-loading in high power Yb-doped fiber amplifiers," in *IEEE Conf.: CLEO: Sci. and Innov.* (2020).
44. J. Jasapara et al., "Effect of heat and H2 gas on the photo-darkening of Yb^{3+} fibers," in *Conf. Lasers and Electro-Opt. Quantum Electron. and Laser Sci. Conf.*, INSPEC Accession Number, p. 10363283 (2006).
45. M. S. Kuznetsov et al., "Electronic and thermal refractive index changes in ytterbium-doped fiber amplifiers," *Opt. Express* **21**, 22374–22388 (2013).
46. S. Yoo et al., "Photodarkening in Yb-doped aluminosilicate fibers induced by 488 nm irradiation," *Opt. Let.* **32**, 1626–1628 (2007).

47. J. Koponen et al., "Photodarkening rate in Yb-doped silica fibers," *App. Opt.* **47**, 1247–1256 (2008).
48. J. J. Koponen et al., "Photodarkening in ytterbium-doped silica fibers," *Proc. SPIE* **5990**, 599008 (2005).
49. F. Mady et al., "Radiation effects in ytterbium-doped silica optical fibers: traps and color centers related to the radiation-induced optical losses," in *RADECS 2010 Proc.*, p. LN2 (2010).
50. M. Engholm et al., "Improved photodarkening resistivity in ytterbium-doped fiber lasers by cerium codoping," *Opt. Lett.* **34**, 1285–1287 (2009).
51. C. Jauregui et al., "Thermal analysis of Yb-doped high-power fiber amplifiers with Al:P co-doped cores," *Opt. Express* **16**, 15540–15545 (2018).
52. S. Taccheo et al., "Concentration dependence and self-similarity of photodarkening losses induced in Yb-doped fibers by comparable excitation," *Opt. Express* **19**, 19340–19345 (2011).
53. T. Sun et al., "Progress and summary of photodarkening in rare earth doped fiber," *Appl. Sci.* **11**, 10386 (2021).
54. L. Xiao et al., "An approximate analytic solution of strongly pumped Yb-doped double-clad fiber lasers without neglecting the scattering loss," *Opt. Commun.* **230**, 401–410 (2004).
55. P. Leproux and S. Février, "Modeling and optimization of double-clad fiber amplifiers using chaotic propagation of the pump," *Opt. Fiber Technol.* **7**, 324–339 (2001).
56. D. Kouznetsov and J. V. Moloney, "Highly efficient, high-gain, short-length, and power-scalable incoherent diode slab-pumped fiber amplifier/laser," *IEEE J. Quantum Electron.* **39**, 1452–1461 (2003).
57. M. Leich et al., "Non-isothermal bleaching of photodarkened Yb-doped fibers," *Opt. Express* **17**, 12588–12593 (2009).
58. P. Yan et al., "Fiber core mode leakage induced by refractive index variation in high-power fiber laser," *Chin. Phys. B* **26**, 034205 (2017).
59. J. Li et al., "Theoretical analysis of the heat dissipation mechanism in Yb^{3+}-doped double-clad fiber lasers," *J. Mod. Opt.* **55**, 459–471 (2008).
60. J. Li et al., "Theoretical analysis and heat dissipation of mid-infrared chalcogenide fiber Raman laser," *Opt. Commun.* **284**, 1278–1283 (2011).
61. M. Sabaeian et al., "Thermal effects on double clad octagonal Yb:glass fiber laser," *Opt. Mater.* **31**, 1300–1305 (2009).
62. P. Yan, A. Xu, and M. Gong, "Numerical analysis of temperature distributions in Yb-doped double-clad fiber lasers with consideration of radiative heat transfer," *Opt. Eng.* **45**, 124201 (2006).

Maryam Karimi received her BSc and MSc degrees from K. N. Toosi University of Technology and from Tarbiat Modares University, Tehran, Iran, in 1998 and 2001, respectively. she joined Iran Telecom Research Center as researcher member until 2005. She received her PhD from Razi University, Kermanshah, Iran, in 2010. Currently, she is the faculty member of Photonic and Quantum Technology Research School, Nuclear Science and Technology Research Institute. Her research interests include in linear and non-linear effects in optical devices and fiber optic equipment.